

## **A SIMPLE PROCESSING APPROACH FOR HOLOGRAPHIC RASCAN DATA**

**F. Soldovieri**

Institute for Electromagnetic Sensing of the Environment  
Via Diocleziano 328, I-80124 Napoli, Italy

**A. F. Morabito and F. D'Agostino**

Dipartimento di Informatica, Matematica, Elettronica e Trasporti  
University 'Mediterranea' of Reggio Calabria  
Via Graziella, Loc. Feo di Vito, I-89124 Reggio Calabria, Italy

**S. I. Ivashov, V. V. Razevig, and I. A. Vasiliev**

Remote Sensing Laboratory  
Bauman Moscow State Technical University  
2nd Baumanskaya Street, 5, 105005 Moscow, Russia

**Abstract**—This paper presents a reconstruction approach which exploits the field detected by a holographic radar in order to localize and geometrically qualify a set of scattering objects. In particular, thanks to the adoption of the Kirchhoff Approximation, the problem is formulated as a linear inverse one wherein the unknown function is the characteristic function accounting for the support (location and geometry) of the target(s). The reconstruction performances of the approach are investigated through an accurate numerical analysis, and an experimental validation is also performed with the aim of testing the effectiveness and the practical relevance of the proposed method.

### **1. INTRODUCTION AND MOTIVATIONS**

The employ of holographic radar is well assessed in literature as imaging and diagnostic tool for hidden objects detection and localization in shallow layers, with applications ranging from material

and civil engineering to ground probing (e.g., to detect buried landmines) [1–3].

Holographic radars exhibit some differences in the working principle compared to the usual time-domain pulsed radar. In fact, the classical time-domain radar works by [4]

1. emitting a UWB (Ultra-wideband) signal;
2. collecting by a receiving antenna the backscattered signal reflected by the heterogeneities present in the investigated medium;
3. achieving information on the targets embedded in the investigated medium by visualizing and processing the backscattered signal collected in the previous step.

Differently, the holographic radar works by transmitting a continuous wave (single tone) at several frequencies [2], so that the data collected by the system are in the spatial and frequency domains [2]. In particular, the collected signal (which is used in the subsequent stages of processing and/or visualization) arises as an ‘interference signal’ mathematically given by the product of the field scattered by the targets and the reference field deriving by the direct coupling between the transmitting and receiving antennas [4].

Moreover, whereas the time-domain impulse radar works by emitting a continuous frequency spectrum, the holographic radar emits a discrete set of frequencies. In particular, the choice of the operating frequency band and of the number of frequencies is dictated by the necessity to provide a sufficient electromagnetic contrast (at least at one of the operating frequencies) between object and embedding medium [1–3]. In fact, for each single working frequency, “blind” depths arise where the sensitivity of the holographic subsurface radar appears to be minimal, due to the non constructive interference [1].

Compared to time-domain impulse radars, holographic radars, by working with discrete spectra, are much easier to be adapted to regulations and demands due to electromagnetic compatibility [5]. Moreover, the use of multi-frequency signal provides good performances in terms of noise rejection.

Another important advantage of holographic radar technology is the possibility to image without reverberation dielectric materials that lie above (or even directly on) a metal surface. Such materials cannot currently be inspected non-destructively with traditional time-domain impulse radar technology. In fact, the reverberation of pulses between the radar antenna and shallow metal objects obscures the actual location and the shape of the objects, while the object is lost in the multiple reflections (often called ‘ghosts’ or ‘phantoms’) of the transmitted impulse signal [6]. The capability of holographic radar to

image objects located over metal surfaces could be very important, f.i. for inspection of the heat protection systems of space ships [2].

Despite of the advantages offered by the hardware, one of the main limitations arising in the use of the holographic radar is the lack of an accurate modeling of the electromagnetic scattering, which is important to set-up inversion approaches able to retrieve the geometry of the targets (especially when the targets are not close to the measurement plane over which the radar system moves, — see [7] for more details on this issue).

As a crucial circumstance, no investigation of the resolution limits of the holographic radar system has been faced. Moreover, it is worth nothing that there is an essential distinction of the term “spatial resolution” between holographic radars and classical impulse radars. For holographic radars this term is accounted for the point spread function over the plane of view at a constant depth (i.e., at a constant distance between the measurement and the object plane). As matter of fact, the spatial resolution is dependent on the depth of the plane of view, on the pattern of the transmitting antenna, and on the working frequency. Even, there is a considerable influence of microwave attenuation in the surveying medium on quality of recorded holograms [8].

In this paper, the problem of the localization and the geometry determination of the targets by holographic radar data in the framework of the linear inverse scattering problem [9] is investigated. In particular, the formulation of the reconstruction problem as a linear inverse one is achieved by means of the adoption of the Kirchhoff Approximation (see [10, 11]). By using a linear formulation, the inverse problem is solved by exploiting the assessed tool of the Singular Value Decomposition [12], which permits to set-up stable inversion schemes and also to investigate their reconstruction performances [12–15].

The paper is organized as follows. Section 2 is devoted at presenting the formulation of the forward problem. In Section 3, the corresponding inverse problem is stated as a linear one, and the reconstruction approach is described. Finally, in Section 4 and Section 5 an analysis with synthetic data and an accurate experimental validation of the reconstruction approach are presented, respectively. Conclusions follow.

## 2. PROBLEM FORMULATION

The transmitting/receiving antenna system plays a key-role in all the ground penetrating radar applications [16, 17]. In order to introduce the approach at hand, let us assume that the antenna system is

deployed under a multi-monostatic configuration (i.e., the location of the transmitting antenna coincides with the measurement point) and moves over a scanning plane at  $z = 0$  while radiating a monochromatic wave.

In particular, we assume a transmitting antenna defined as a rectangular aperture with an aperture field having an uniform tangential field  $E_0$  directed along the  $y$ -axis. By applying the *Equivalence Theorem* [18], it is easy to prove that the electromagnetic field radiated by such an aperture in the half-space  $z > 0$  is the same as the field radiated by the equivalent magnetic surface density current  $\vec{J}_m = 2E_0\hat{x}$  having support on the aperture. Now, we make the further simplifying hypothesis that the sides of the aperture are small in terms of the radiated wavelength and denote with  $A$  the area of the aperture.

The choice of the uniform aperture field is justified on the basis of the considerations made in [7] and by the fact that we are now considering as antenna an elementary source. Such an elementary source gives us the possibility to account more complicated sources since the formulation below will remain the same with the only exception that the radiated field is expressed under an integral form.

Therefore, by denoting with  $R = \sqrt{(x - x')^2 + (y - y')^2 + z^2}$  the distance between the observation point [located at the point  $(x, y, z)$ ] and the magnetic dipole point [located at the coordinates  $(x', y', 0)$ ], the transverse components of the radiated magnetic field are given by

$$H_x(x, y, z) = S(f)2E_0A[(\beta^2/R) - \beta^2(x - x')^2/R^3] \exp(-j\beta R) \quad (1a)$$

$$H_y(x, y, z) = S(f)2E_0A[-\beta^2(x - x')(y - y')/R^3] \exp(-j\beta R) \quad (1b)$$

Note that in (1a) and (1b) we have retained the only terms of the radiated field that behave as  $1/R$ ; in other words, we neglect in the expression of the radiated magnetic field the terms that go to zero in a faster way compared to the dependence  $1/R$ .  $S(f) = -j/(4\pi\omega\mu_0)$  is a term only-frequency dependent, wherein  $j$  is the imaginary unit and  $\omega = 2\pi f$  (being  $f$  the working frequency);  $\beta$  and  $\mu_0$  represent the wave-number of the investigated medium and the magnetic permeability in free space, respectively.

We assume that the objects to be investigated have a planar shape and dimensions comparable with the probing wavelength, and that they are located in a plane at constant depth  $\tilde{z}$ ; under these assumptions, it is possible to exploit the Kirchhoff Approximation [10, 11] and to write the electric density current induced on the target's surface as

$$\begin{aligned} \vec{J}_{opt} &= 2\hat{n} \times \vec{H}_i = -2\hat{z} \times (H_x\hat{x} + H_y\hat{y}) \\ &= -2H_xU(x, y)\delta(z - \tilde{z})\hat{y} + 2H_yU(x, y)\delta(z - \tilde{z})\hat{x} \end{aligned} \quad (2)$$

wherein  $\hat{n} = -\hat{z}$  is the normal to the targets' surfaces and  $\vec{H}_i$  is the incident magnetic field. The geometry of the targets is accounted by  $U(x', y')$ , which is the unknown characteristic function accounting for the illuminated surface of the target, and  $\delta(\cdot)$  is the Dirac delta function.

The two components of the induced electric current in Eq. (2) give rise to the scattered field, which is evaluated in the same point of the source  $(x', y', 0)$ ; for the scattered field we consider only the  $y$ -component given by the sum of two contributions:

- a first contribution radiated by the  $y$ -component of the electric current in Eq. (2), i.e.,

$$E_{1_{sy}} = S(f)S_1(f) \int_V -2E_0A[(\beta^2/R) - \beta^2(x - x')^2/R^3] [(\beta^2/R) - \beta^2(y - y')^2/R^3] \exp(-2j\beta R)U(x, y)\delta(z - \tilde{z})dxdy \quad (3a)$$

- a second contribution radiated by the  $x$ -component of the electric current in Eq. (2), i.e.,

$$E_{2_{sy}} = S(f)S_1(f) \int_V 2E_0A[-\beta^2(x - x')(y - y')/R^3] [-\beta^2(y - y')(x - x')/R^3] \exp(-2j\beta R)U(x, y)\delta(z - \tilde{z})dxdy \quad (3b)$$

wherein  $S_1(f) = -j/(4\pi\omega\varepsilon_0)$ .

By considering the constant term  $C_0e^{j\varphi_0}$  as reference field and taking into account the real part of the 'interference' of the scattered field with such a reference field, finally we obtain the datum of the problem as

$$E_{sx} = S(f)S_1(f) \int_V 2C_0E_0A \left\{ \begin{aligned} &[-\beta^2(x - x')(y - y')/R^3][-\beta^2(y - y')(x - x')/R^3] + \\ &-[(\beta^2/R) - \beta^2(x - x')^2/R^3][(\beta^2/R) - \beta^2(y - y')^2/R^3] \end{aligned} \right\} \cos(2\beta R + \varphi_0)U(x, y)\delta(z - \tilde{z})dxdy \quad (4)$$

that can be rearranged as

$$E_{sx} = -S(f)S_1(f) \int_V 2E_0C_0A \{ [(\beta^2/R)][(\beta^2/R) - \beta^2(x - x')^2/R^3 - \beta^2(y - y')^2/R^3] \} \cos(2\beta R + \varphi_0)U(x, y)\delta(z - \tilde{z})dxdy \quad (5)$$

Therefore, the problem at hand can be cast as the determination of the unknown characteristic function  $U(x, y)$  (accounting for the location and geometry of the target) at depth  $\tilde{z}$  starting from the scattered field datum  $E_{sx}$  given in Eq. (5).

### 3. THE RECONSTRUCTION APPROACH

As it was mentioned above, the problem at hand is formulated as the inversion of the linear integral Eq. (5), which connects the unknown characteristic function at the depth  $\tilde{z}$  to the interference signal.

Such an inversion is performed by means of the Singular Value Decomposition (SVD) [12, 13] of the operator defined by Eq. (5), which provides the singular system  $\{\sigma_n, u_n, v_n\}_{n=0}^{\infty}$ , wherein the set  $\{\sigma_n\}_{n=0}^{\infty}$  denotes the sequence of the singular values ordered in a decreasing sequence while  $\{u_n\}_{n=0}^{\infty}$  and  $\{v_n\}_{n=0}^{\infty}$  form the basis for the space of the visible objects (i.e., the objects that could be retrieved by the error-free data) and for the closure of the range of the operator, respectively.

As a crucial circumstance, the analysis of the singular values of the operator at hand (see Fig. 1) allows to state the ill-posedness [13] of the inverse problem. In particular, for three different distances between the measurement plane and the investigation plane (depths 0.02 m, 0.2 m, and 2 m), Fig. 1 depicts the normalized amplitude of the singular values in the case of a measurement domain with side  $s = 0.48$  m (where the measurements are collected at a step of 0.02 m). The investigation

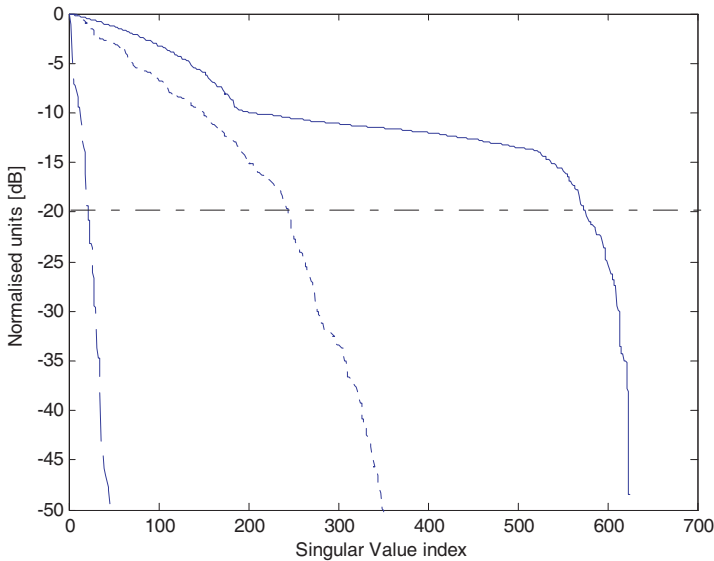


**Figure 1.** Behaviour of the singular values of the operator at hand for different distances between the measurement and the investigation planes:  $d = 0.02$  m, solid line;  $d = 0.2$  m, dotted line;  $d = 2$  m, dashed line.

plane (wherein the target is assumed to reside) has the same extent of the measurement plane. The work frequency is  $f = 3$  GHz.

The numerical investigation of the singular values (see Fig. 1) allows us to point out how the information content (given as the number of significant singular values) increases as long as the distance between the measurement plane ( $z = 0$ ) and the investigation plane decreases.

Because of the exponential decay of the singular values, the Truncated SVD (TSVD) expansion [13] has been adopted as regularization scheme, and the following regularized solution has been considered:

$$\gamma = \sum_{n=0}^N \frac{1}{\sigma_n} \langle E_s, v_n \rangle u_n \quad (6)$$

where  $\langle \cdot, \cdot \rangle$  denote the scalar product in the data space.

By restricting the solution space to the one spanned by the first  $N+1$  singular functions  $\{u_n\}_{n=0}^{\infty}$ , the TSVD regularization scheme does not amplify the effect of errors and uncertainties on data, so that the solution is made stable. The choice of the index  $N$  has to be performed with regard to ‘the degree of regularization’ one wants to achieve in the inversion also in dependence of the *signal to noise ratio* [13].

It is worth nothing that the SVD tool permits to investigate also the performances of the reconstruction approach in terms of the regularized point spread function in dependence on the level of truncation in the SVD and on the parameters of the geometry (as shown in [14, 15]).

#### 4. RECONSTRUCTION PERFORMANCES OF THE IMAGING APPROACH

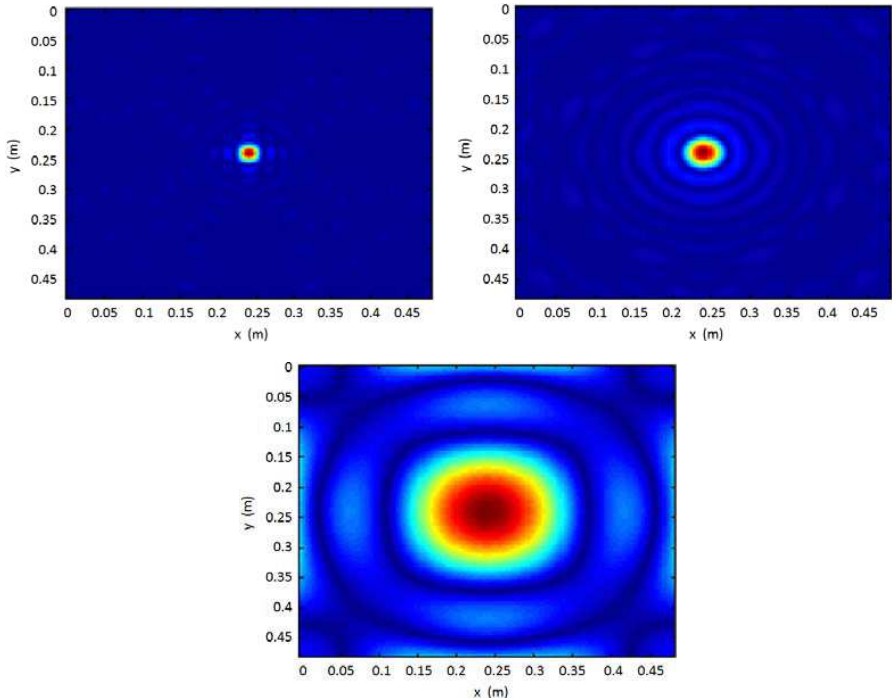
This section is devoted at presenting the performances of the reconstruction approach in dependence on the parameters of the measurement configuration and of the effects of different quantities and uncertainties.

In particular, a test case where the measurements are collected with a spatial step  $d = 0.02$  m over a finite square domain of side  $s = 0.48$  m located at the plane  $z = 0$  is considered. The working frequency is  $f = 3$  GHz. The investigation plane (within which the target is assumed to reside) has the same extent of the measurement plane. Different studies and issues are addressed in the following Subsections.

#### 4.1. The Effect of the Regularization Parameter and of the Distance between the Planes in TSVD Scheme

In this Subsection, the case of the different thresholds (truncation index  $N$ ) exploited in the TSVD scheme is presented [see Eq. (6)]. In particular, a number of numerical experiments have been performed by varying the parameter  $f_{reg}$ , which represents the minimum singular value considered in the TSVD regularization normalized to the maximum singular value. Initially, assumption that the data are not affected by noise has been done, and the reconstruction results are given in terms of the modulus of the function  $\gamma$  retrieved by the TSVD scheme [see Eq. (6)].

The reconstructions presented below are concerned with a point target located at the center of the measurement plane, i.e.,  $x = y = 0$ .



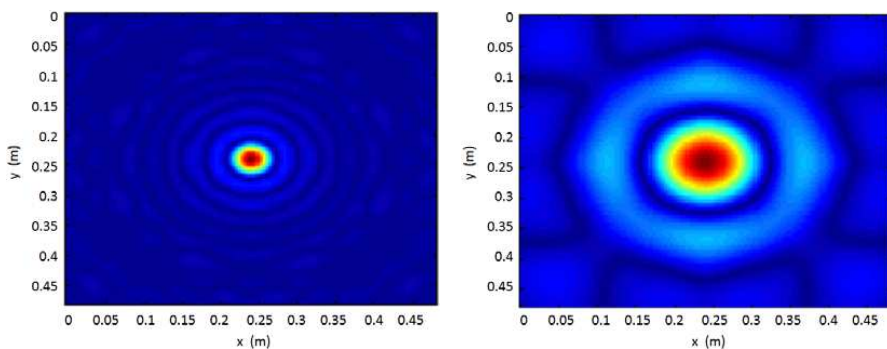
**Figure 2.** Reconstruction (amplitude of the characteristic function) of the target point with regularization parameter  $f_{reg} = 0.1$  at different distances between the investigation plane and the measurement plane:  $d = 0.02$  m (left panel),  $d = 0.2$  m (right panel), and  $d = 2$  m (bottom panel).

Figure 2 shows the reconstruction of the point target for the three different distances between the measurement plane and the target (investigation) plane. In the TSVD scheme, only the terms corresponding to the singular values larger than  $f_{reg} \cdot \sigma_0$  have been retained, wherein  $\sigma_0$  is the first and largest singular value and  $f_{reg}$  is a regularization parameter which has to be properly chosen by the user. In this Subsection, the choice  $f_{reg} = 0.1$  has been performed.

The three reconstructions are concerned with the depths  $d = 0.02$  m,  $d = 0.2$  m, and  $d = 2$  m, and allow to point out how the achievable resolution worsens as the depth increases. This is coherent with the singular values behaviour of Fig. 1. In fact, if the distance between the planes increases, then the number of singular values larger than  $f_{reg} \cdot \sigma_0$  decreases and, accordingly, the resolution deteriorates.

In Fig. 3, the effect of the threshold  $f_{reg}$  adopted in the TSVD as far as the resolution limits is shown. In particular, for the case  $d = 0.2$  m, besides the above presented case (i.e., threshold  $f_{reg} = 0.1$ ), the result with  $f_{reg} = 0.9$  is reported in order to prove that a stronger degree of the regularization entails a loss of resolution.

Finally, the case concerned with the effect of the error in the knowledge of the depth of the target (i.e., distance between the planes) has been considered. In particular, in the inversion model a distance between the planes  $d = 0.2$  m has been imposed, whereas the two considered datasets have been generated by considering respectively the actual depth equal to 0.1 m and 0.3 m. The two reconstruction results are reported in Fig. 4 and allows one to state that an inaccurate knowledge of the depth of the targets induces a defocusing effect in the reconstruction.



**Figure 3.** Reconstruction (amplitude of the characteristic function) of the target point at distance  $d = 0.2$  m with different TSVD thresholds:  $f_{reg} = 0.1$  left panel;  $f_{reg} = 0.9$  right panel.

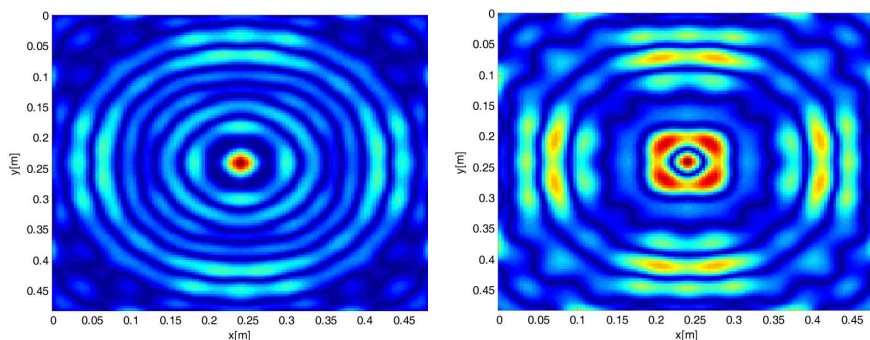


**Figure 4.** Reconstruction (amplitude of the characteristic function) of the target point at  $d = 0.2$  m when the depth of the investigation plane is erroneously accounted for in the inversion model:  $d = 0.1$  m, left panel;  $d = 0.3$  m, right panel.

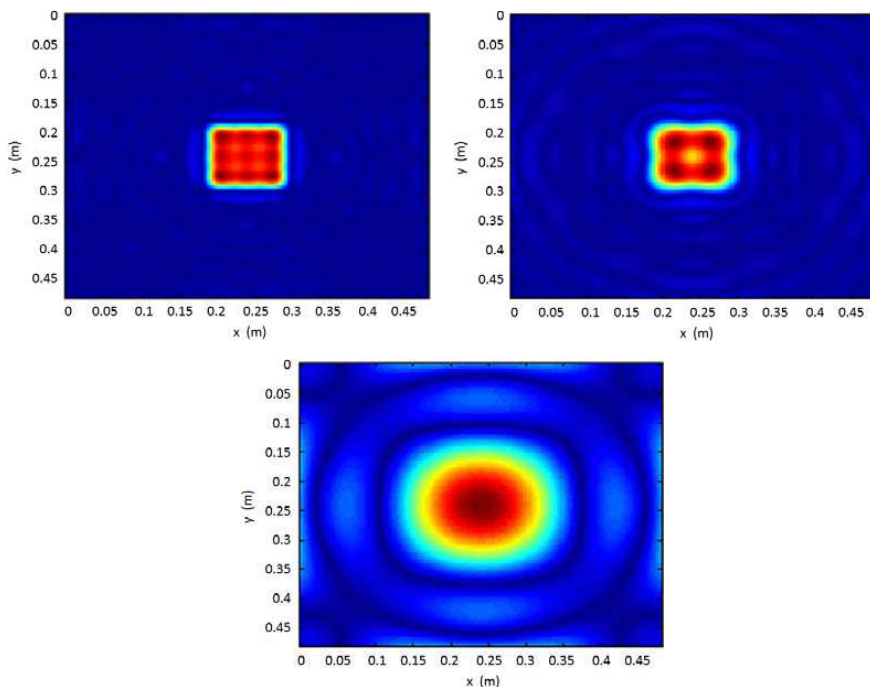


**Figure 5.** Reconstruction (amplitude of the characteristic function) of an extended object with  $freq = 0.1$  at different distances between the investigation plane and the measurement plane:  $d = 0.02$  m (left panel),  $d = 0.2$  m (right panel), and  $d = 2$  m (bottom panel).

## 4.2. Reconstruction of an Extended Object

This subsection is devoted at presenting reconstruction results for a square object of side  $s = 0.08$  m. Once a threshold  $f_{reg} = 0.1$  has been fixed in the TSVD scheme, a number of numerical experiments have been performed by varying the distance between the two planes. The achieved results, which are shown in Fig. 5, prove that an increasing of such a distance induces a worsening of the reconstruction. However, the contour of the object is clearly identified for the depths  $d = 0.02$  m and  $d = 0.2$  m, while in the case  $d = 2$  m it is still possible to detect the target and roughly determine the shape.

As a final assessment of the proposed approach, the reconstruction procedure has been performed by starting from noisy data. Fig. 6 shows the results achieved by considering data with a Signal to Noise Ratio  $SNR = 0.7$  and exploiting  $f_{reg} = 0.1$  in the TSVD scheme. As it can be seen, despite of the very low SNR, the approach is still able to detect and roughly determine the extent of the object.

## 5. RECONSTRUCTION RESULTS FROM EXPERIMENTAL DATA

This section is devoted at presenting the results of the application of the proposed processing approach to experimental data. In particular, a subset of the measurements presented in [7] has been used to evaluate the performances of the approach.

The experiment is concerned with a sheet of paper where embedded letters was constructed.

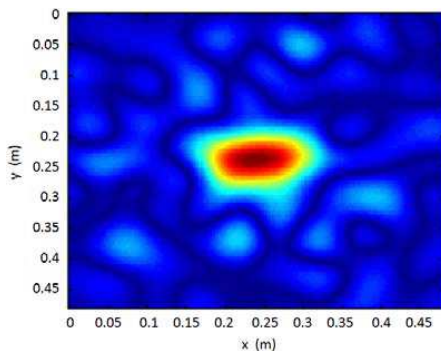


**Figure 6.** Reconstruction (amplitude of the characteristic function) of an extended object with  $f_{reg} = 0.6$  and  $SNR = 0.7$ .



**Figure 7.** Application of the proposed processing approach to experimental data: Photo of the investigated object.

The letters were cut from a thin aluminium foil. The dimensions of the word 'RASCAN' are 44 cm by 11.5 cm, as shown in Fig. 7. The paper sheet with aluminium lettering was placed on a plaster sheet, and it was covered by other plaster sheets one-by-one. The single plaster sheet has a thickness equal to 1.2 cm and relative dielectric permittivity  $\varepsilon = 2.41$  F/m. After addition of each new sheet to the stack, the hidden paper sheet was scanned by hand using the RASCAN-4/4000 radar. Every scan included simultaneous recording of ten radar holograms, at each of five discrete frequencies, with two polarizations per frequency. The dimensions of scanned area were equal to 65 cm by 28 cm.

A minimal training of the operator has been required to properly record the RASCAN radar holograms. In particular, holograms were recorded as individual raster or scanning lines along which the radar head was swept by hand. In order to avoid distortion of the image, these lines were parallel and equidistant.

The time required for the scanning procedure depended on the dimensions of the area and on the selected step between raster lines. Measurements collected with a step of length  $l = 0.5$  cm along the two directions were exploited, so that a rectangular measurement grid with a uniform spacing distance was considered.

The numerical experiments are concerned with a working frequency  $f = 3.85$  GHz, and different numbers of plaster sheets covering the target. In particular,

- the first result is concerned with the case of two sheets covering the target (so that the thickness of the plaster sheets is equal to 2.4 cm);
- the second result is concerned with the case of four sheets covering the target (so that the thickness of the plaster sheets is equal to 4.8 cm);
- the third result is concerned with the case of six sheets covering the target (so that the thickness of the plaster sheets is equal to 7.2 cm).

For each of these experiments, Figs. 8–10 compare the data used in the inversion with the reconstruction result in terms of amplitude of the retrieved characteristic function.

In the case wherein a number of sheets larger than three has been adopted, the outlines of letters have become more blurred, and the images have exhibited a wavy nature. These phenomena are readily explained: at very shallow depths, there is direct reflection in nadir from surface of the letters with very high level of reflected signal (higher than the level of the reference one and higher than off-nadir reflections).

The comparison between the data and the reconstruction makes it possible to point out, especially for the first and third experiment

(see Figs. 8 and 10), that the reconstruction results are more easily interpretable and cleaner compared to the data. Differently, these good performances do not arise for the second experiment (see Fig. 9), where the quality of data is not suitable to achieve a reconstruction result of quality comparable to the ones of the other two experiments.

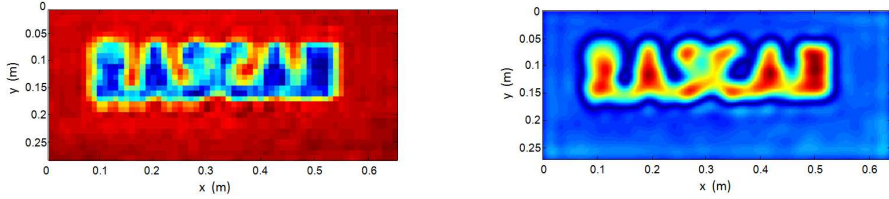


**Figure 8.** First reconstruction result from experimental data ( $d = 2.4$  cm): Comparison (in terms of amplitude of the characteristic function) between the data used in the inversion (left panel) and the reconstruction result (right panel).

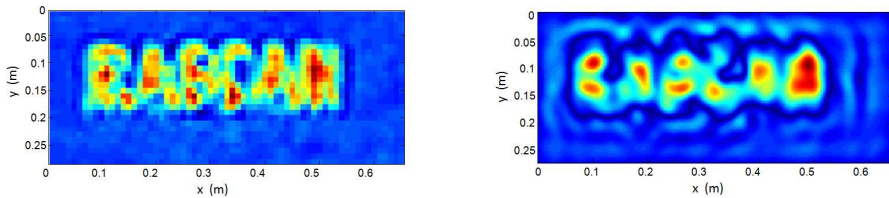


**Figure 9.** Second reconstruction result from experimental data ( $d = 4.8$  cm): Comparison (in terms of amplitude of the characteristic function) between the data used in the inversion (left panel) and the reconstruction result (right panel).

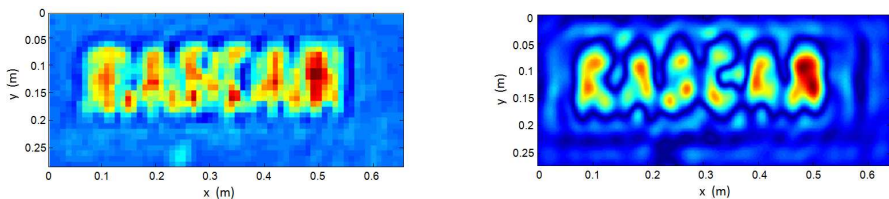


**Figure 10.** Third reconstruction result from experimental data ( $d = 7.2$  cm): Comparison (in terms of amplitude of the characteristic function) between the data used in the inversion (left panel) and the reconstruction result (right panel).

## 6. CONCLUSION

This paper has presented a simple inversion approach for the problem of imaging embedded targets thanks to holographic radar data. A linear inversion approach has been implemented under the hypothesis of Kirchhoff Approximation and by exploiting as solution tool the Singular Values Decomposition of the relevant operator. The TSVD has permitted us to outline the performances of the inversion approach in dependence of some factors as: the distance between the measurement plane and the investigation plane (and/or its non-accurate knowledge), the degree of regularization in the inverse problem, the presence of noise on the input data.

Moreover, experimental data sets recorded by subsurface radar of RASCAN type were used in order to test the effectiveness of the proposed procedure. It has been shown that the restored holograms give better resolution in comparison with original microwave images.

As future developments of the research activity, we will address the problem of the determination of the depth of the targets by exploiting the multi-frequency information collected by the system.

## ACKNOWLEDGMENT

The research leading to these results has received funding from the European Community's Seventh Framework Programme (FP7/2007-2013) under Grant Agreement No. 225663 Joint Call FP7-ICT-SEC-2007-1.

## REFERENCES

1. Ivashov, S., V. Razevig, I. Vasilyev, A. Zhuravlev, T. Bechtel, and L. Capineri, "The holographic principle in subsurface radar technology," *International Symposium to Commemorate the 60th Anniversary of the Invention of Holography*, 183–197, Springfield, Massachusetts, USA, October 27–29, 2008.
2. Ivashov, S. I., I. A. Vasiliev, T. D. Bechtel, and C. Snapp, "Comparison between impulse and holographic subsurface radar for NDT of space vehicle structural materials," *PIERS Online*, Vol. 3, No. 5, 658–661, 2007.
3. Case, J. T., J. Robbins, S. Kharkovsky, F. Hepburn, and R. Zoughi, "Microwave and millimeter wave imaging of the space shuttle external fuel tank spray on foam insulation (SOFI) using synthetic aperture focusing techniques (SAFT)," CP820, *Review of Quantitative Nondestructive Evaluation*, D. O. Thompson and

- D. E. Chimenti (eds.), Vol. 25, American Institute of Physics, 2006.
4. Daniels, D. J., *Surface-penetrating Radar*, IEE, London, 1996.
  5. Dennis, J., *GPR — The Impact of New FCC Regulations*, GSSI, July 25, 2002.
  6. Chapursky, V. V., S. I. Ivashov, V. V. Razevig, A. P. Sheyko, I. A. Vasilyev, V. V. Pomozov, N. P. Semeikin, and D. J. Desmond, "Subsurface radar examination of an airstrip," *Proceedings of the 2002 IEEE Conference on Ultra Wideband Systems and Technologies, UWBST'2002*, 181–186, Baltimore, Maryland, USA, May 20–23, 2002.
  7. Chapursky, V. V., S. I. Ivashov, V. V. Razevig, A. P. Sheyko, and I. A. Vasilyev, "Microwave hologram reconstruction for the RASCAN type subsurface radar," *Proceedings of the Ninth International Conference on Ground Penetrating Radar, GPR'2002*, 520–526, Santa Barbara, California, USA, April 29–May 2, 2002.
  8. Razevig, V. V., S. I. Ivashov, I. A. Vasiliev, A. V. Zhuravlev, T. Bechtel, and L. Capineri, "Advantages and restrictions of holographic subsurface radars. Experimental evaluation," *XIII International Conference on Ground Penetrating Radar, GPR 2010*, Lecce, Italy, June 21–25, 2010.
  9. Solimene, R., A. Brancaccio, R. Pierri, and F. Soldovieri, "Two experimental results by a linear inverse scattering approach," *Progress In Electromagnetics Research*, Vol. 91, 259–272, 2009.
  10. Bourlier, C., H. He, J. Chauveau, R. Hémon, and P. Pouliguen, "RCS of large bent waveguide ducts from a modal analysis combined with the Kirchhoff approximation," *Progress In Electromagnetics Research*, Vol. 88, 1–38, 2008.
  11. Soldovieri, F., A. Brancaccio, G. Prisco, R. Pierri, and G. Leone, "A Kirchhoff-based shape reconstruction algorithm for the multimonostatic configuration: The realistic case of buried pipes," *IEEE Transactions on Geoscience and Remote Sensing*, Vol. 46, No. 10, 3031–3038, 2008.
  12. Bertero, M. and C. de Mol, "SVD for linear inverse problems," *SVD and Signal Processing III*, M. Moonen and B. de Moor (eds.), 341–348, Elsevier, Amsterdam, 1995.
  13. Bertero, M., "Linear inverse and ill-posed problems," *Advances in Electronics and Electron Physics*, Vol. 75, 1–114, Academic Press, 1989.
  14. Pierri, R., A. Lisenò, and F. Soldovieri, "Shape reconstruction

- from PO multifrequency scattered fields via the singular value decomposition approach,” *IEEE Transactions on Antennas and Propagation*, Vol. 49, No. 9, 1333–1343, 2001.
15. Lee, K.-C., J.-S. Ou, and M.-C. Fang, “Application of SVD noise-reduction technique to PCA based radar target recognition,” *Progress In Electromagnetics Research*, Vol. 81, 447–459, 2008.
  16. Romano, N., G. Prisco, and F. Soldovieri, “Design of a reconfigurable antenna for ground penetrating radar applications,” *Progress In Electromagnetics Research*, Vol. 94, 1–18, 2009.
  17. Soldovieri, F. and N. Romano, “The mutual interaction between the reconfigurable transmitting and receiving antennas in ground penetrating radar surveys,” *Journal of Electromagnetic Waves and Applications*, Vol. 23, No. 14–15, 1919–1928, 2009.
  18. Balanis, C. A., “Field equivalence principle — Aperture antennas,” *Antenna Theory: Analysis and Design*, 3rd edition, 653–662, John Wiley & Sons, Publishers, Inc., New York, 2006.